光学学报

闪耀型亚波长光栅透镜的柱矢量光聚焦优化和调控

王俊[1]，许吉[1*]，李胜[1]，迟甜甜[1]，姚晗[1]，张柏富[2]，刘宁[1]

[1]南京邮电大学电子与光学工程学院、柔性电子（未来技术）学院，江苏 南京 210023；
[2]南京理工大学电子工程与光电技术学院，江苏 南京 210023

摘要 柱矢量光束的紧聚焦在光学微操纵、光学存储、激光微加工、超分辨率成像和粒子加速等领域发挥着重要作用。亚波长光栅平凹透镜对柱矢量光束的紧聚焦的能力仍有提升空间，本文利用闪耀结构将光的能量从零级转移并集中到−1级，对亚波长光栅平凹透镜的聚焦性能进行优化。提高了透镜的衍射效率，增强了焦场的能量。通过调整高斯径向偏振光的形状参数，改变入射光振幅及入射区域半径实现对焦场能量的动态调控。进一步地，调控柱矢量光束的偏振组分能够直接有效地横向调制焦场，获得多样化形貌的焦斑。本文的优化手段对于其他光栅透镜也具有参考意义，该研究结果在超分辨率成像以及光场调控等领域具有潜在的应用价值。

关键词 亚波长光栅透镜；柱矢量光束；闪耀结构；聚焦；调控

1 引　　言

柱矢量光束（CVBs）的振幅和偏振呈柱对称分布，其紧聚焦在光学微操纵[1-3]、光学存储[4-5]、激光微加工[6-7]、超分辨率成像[8-10]和粒子加速[11-12]等领域发挥着重要作用。目前，已发展出多样化的聚焦手段，既有各自优势又均存在一定的局限性。传统透镜聚焦方法简单，但难以突破衍射极限实现紧聚焦[13]；等离激元透镜可以突破衍射极限聚焦，但等离激元激发的偏振依赖性造成聚焦光束的偏振态局限性[14-15]；负折射光子晶体透镜能突破偏振态限制，但结构复杂制备难度大[16]；抛物面反射镜近轴聚焦可获得长焦深焦场，但焦场受入射光场干扰而应用受限[17-18]；超构透镜通过调整阵列结构可实现多元化的焦场调控，但结构复合度高存在一定设计和制备难度[19-20]。单一介质的亚波长光栅透镜，基于−1级衍射的等效负折射效应，通过结构的优化设计，可实现对径向和旋向偏振光同时有效的紧聚焦，突破衍射极限，焦场与入射光位于透镜异侧，在实现焦场灵活调控的同时，结构易于设计和制备[21]。

基于亚波长光栅透镜的柱矢量光束聚焦，已经取得一系列研究进展[21-24]。级联超材料柱矢量光束发射器与光栅透镜获得柱矢量光场的紧密聚焦特性；对于结构简易的负折射光栅透镜，灵活设计平凹形透镜出

射面轮廓可获得满足预设焦距的单焦点；进一步分区域设计出射面轮廓能够获得双焦点；透镜结构演变为平锥形将获得长焦深焦场。通过优化透镜结构长周期光栅区域，进一步抑制了高级次衍射引起的次级焦点、焦点耦合、焦点偏移等现象。然而，对于负折射光栅透镜，焦场能量效率仍有较大的提升空间。众所周知，光栅衍射光中0级占比极大，会严重削减由−1级衍射光实现聚焦的焦场能量效率，因此需要探索一种能有效提升−1级衍射光能量占比的结构优化方案以增强焦场能量。

闪耀光栅可将大部分衍射光能量集中到某个非零级次，提高其衍射效率[25]。利用该机制，本文将光栅透镜进行闪耀结构的修饰和优化，通过提高−1级衍射光的能量占比以提升聚焦能量效率。利用基于有限元法（FEM）的电磁场全矢量计算（COMSOL Multiphysics 软件）展开了具体研究，比较了闪耀结构修饰前后焦场的能量及形貌变化；分析了闪耀结构的高度、构建数量和位置对于焦场的影响；进一步研究了入射光振幅分布和偏振组分对焦场能量和形貌的动态调控效果。

2 闪耀型亚波长光栅平凹透镜

图1为亚波长光栅平凹透镜修饰闪耀结构的优化

方案。图 1(a)为光栅平凹透镜结构及聚焦示意图。闪耀结构修饰前,已实现高级次衍射抑制的光栅平凹镜为中空型,透镜出射面出现多级衍射,其中具有等效负折射效应的 −1 级衍射在 F 点处满足相长干涉相位条件时,形成聚焦。光栅 −1 级衍射的等效负折射率 n_{eff}[22]为

$$n_{\mathrm{eff}} = n - \lambda_0/d, \tag{1}$$

式中:n 为透镜介质折射率;d 为每个光栅单元(本文中

描述为阶梯)的垂直高度;λ_0 为入射光波长。在 r-z 平面内,每个光栅阶梯顶点的坐标关系[23]满足:

$$n_0^2 r^2 + (n_0^2 - n_{\mathrm{eff}}^2)(z + 3d)^2 - 2n_0(f + 3d)(1 - n_{\mathrm{eff}})(z + 3d) = 0, \tag{2}$$

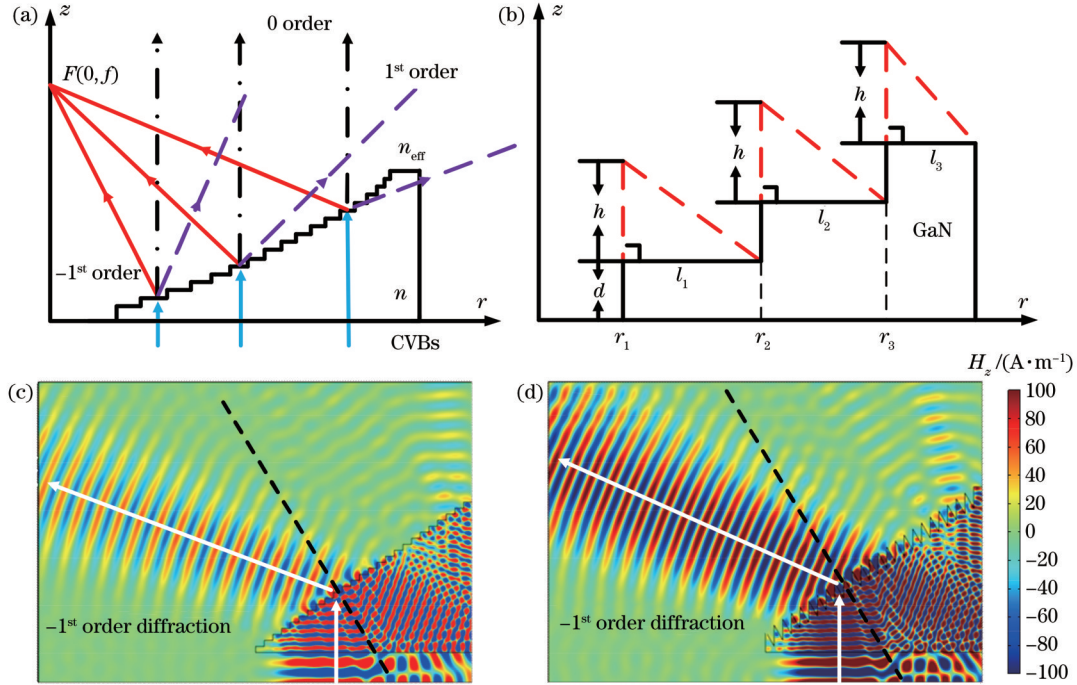式中:f 为预设焦距;r 为径向坐标;z 为纵向坐标。固定 d,每一级阶梯顶点纵坐标高度满足 $z_1 = d, z_2 = 2d, z_3 = 3d, \cdots, z_m = md$,$m$ 为阶梯总个数。

图 1 光栅平凹透镜的优化方案。(a) r-z 截面光栅平凹透镜结构及聚焦示意图;(b)构建闪耀结构示意图;(c)未构建闪耀结构的光栅三棱镜衍射;(d)构建闪耀结构的光栅三棱镜衍射

Fig. 1 Optimization scheme for grating plano-concave lens. (a) Schematic diagram of structure and focusing of grating plano-concave lens in r-z plane; (b) schematic diagram of blazed structure construction; (c) diffraction of grating prism without blazed structure; (d) diffraction of grating prism with blazed structure

出射面光栅修饰闪耀结构方法如图 1(b)所示。闪耀结构位于每一级光栅阶梯上,整体结构为均一介质 GaN,折射率 $n = 2.36$。闪耀结构高度为 h,宽度 l 与每层阶梯宽度一致,第 k 级 l_k 为

$$l_k = r_{k+1} - r_k = [2n_0(f + 3d)(1 - n_{\mathrm{eff}})(z_{k+1} + 3d) - (n_0^2 - n_{\mathrm{eff}}^2)(z_{k+1} + 3d)^2]^{1/2} - [2n_0(f + 3d)(1 - n_{\mathrm{eff}})(z_k + 3d) - (n_0^2 - n_{\mathrm{eff}}^2)(z_k + 3d)^2]^{1/2}。 \tag{3}$$

图 1(c)和 1(d)分别给出了修饰闪耀结构前后的光栅三棱镜模型衍射效应对比。结果表明,构建闪耀结构的 −1 级衍射能量显著增强,意味着 −1 级衍射能量占比的提升,可预期闪耀结构将有效提高负折射光栅平凹镜的聚焦能量效率。

平凹透镜出射面轮廓可等效为一系列不同结构参数三棱镜的连续组合。图 2 为构建闪耀结构前后的径向偏振光焦场对比。选取 $n_{\mathrm{eff}} = -0.9$,$f = 6$ μm,$d = 163.2$ nm,$\lambda_0 = 532.6$ nm,$h = 1.5 d$,$m = 27$。计算并观察透镜优化前后的焦场,即图 2(a)和 2(b),发现优化

后的焦场更明亮。图 2(c)与 2(d)为焦场强度的等高线图,取值范围为 0.5~1.0,描绘出焦场的形貌轮廓,优化后的焦场横向尺寸有较小程度的变宽。图 2(e)是归一化电场强度沿纵向的分布。一方面可以明显看出,闪耀型透镜焦场的能量峰值是优化前的 2.91 倍;另一方面也可发现,闪耀结构的修饰,在原有结构的基础上补偿了中空型透镜焦点位置偏移,实现了更符合预期焦距的聚焦。图 2(f)为归一化电场强度沿横向的分布,优化前后的焦点横向半峰全宽分别为 $0.431\lambda_0$ 和 $0.458\lambda_0$。上述结果表明,闪耀结构的修饰对焦场能量
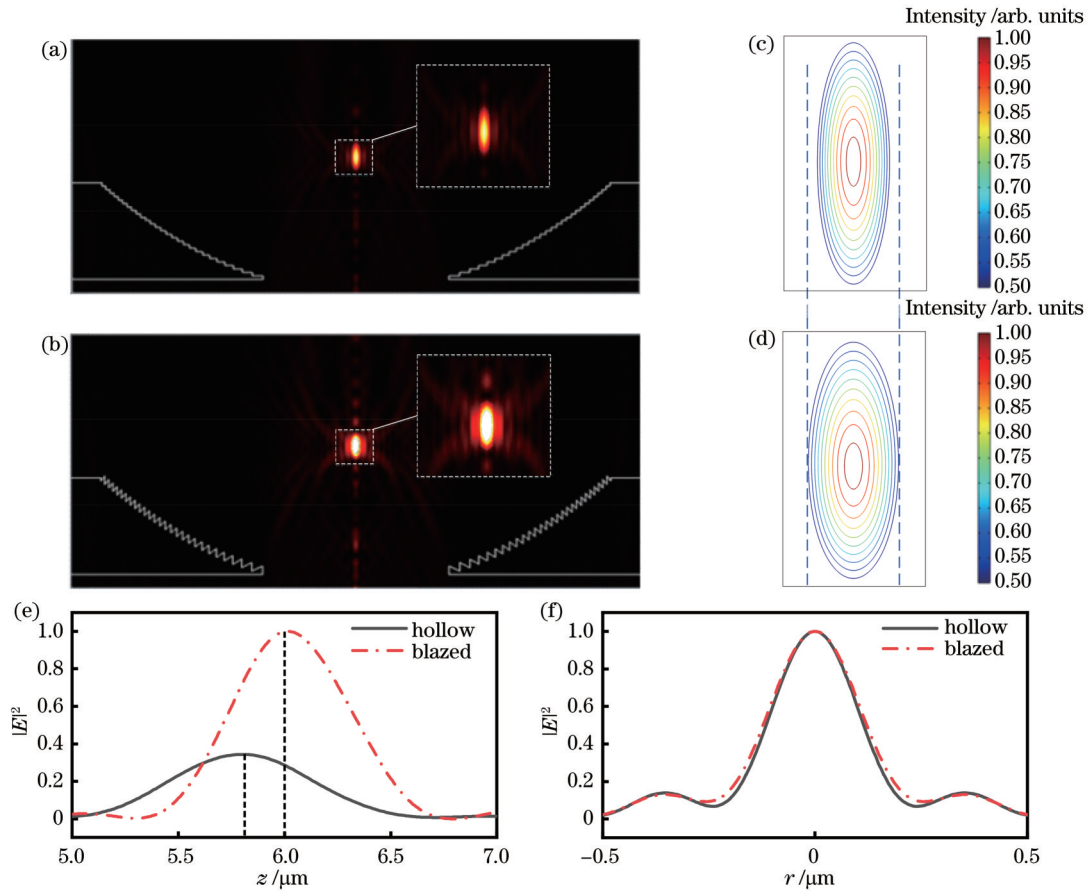
图 2　修饰闪耀结构前后的径向偏振光焦场对比。(a) 中空型和 (b) 闪耀型透镜的焦场图；(c) 中空型和 (d) 闪耀型透镜的焦场强度等高线图；(e) 优化前结构焦场场强峰值归一化的电场强度沿纵向分布；(f) 归一化电场强度沿横向分布

Fig. 2　Comparison of radial polarized light focal fields before and after modifying blazed structure. Focal field distributions of (a) hollow and (b) blazed lenses; focal field intensity contour line diagrams of (c) hollow and (d) blazed lenses; (e) normalized electric field intensity distribution along longitudinal direction based on peak intensity before optimization; (f) normalized electric field intensity distribution along lateral direction

提升具有显著效果，同时对聚焦效果的焦点位置、焦点形貌等也产生了一定影响。

3　闪耀结构参数对聚焦效果的影响

闪耀结构参数密切影响透镜的衍射效率，也将直接影响透镜的聚焦效率和焦场能量。为了便于结构设计和优化，固定每个光栅阶梯上修饰的闪耀结构宽度均与每个光栅阶梯宽度一致，调节闪耀结构高度、数量及位置，探索其对聚焦效果的影响。

3.1　闪耀结构高度的影响

不同的预设焦距，透镜结构的轮廓不同，光束通过透镜的偏折程度也不同，选择 4、6、8 μm 三个典型预设焦距值进行深入讨论。透镜的主体半径大约 8 μm，基于不同预设焦距情况的出射光偏折角程度，定义 4 μm 为近焦距、6 μm 为中焦距、8 μm 为远焦距。图 3 给出了不同焦距情况下，闪耀结构高度 h 从 $0.5d$ 变化至 $2.5d$ 时，径向偏振光焦场能量的增强情况。

图 3(a)～(c) 分别是三个不同预设焦距情况下，焦场依据优化前归一的沿轴向分布图。从图 3(a) 和

3(b) 可以看出，在近焦距和中焦距时，焦场能量随着闪耀结构高度先增加后减小；从图 3(c) 可以看出，在远焦距时，焦场能量随着闪耀结构高度递增。定义闪耀型与中空型透镜焦场能量峰值之比为增强因子 Q：

$$Q = \frac{|E_\mathrm{B}|^2}{|E_\mathrm{H}|^2}。 \tag{4}$$

图 3(d) 为增强因子 Q 随着闪耀结构高度 h 的变化曲线，Q_max 的具体数值如表 1 所示。随着预设焦距增大，增强因子 Q 达到最大值时，所需的闪耀结构高度也随之增加。根据式 (2) 可以判断，预设焦距越大，透镜的出射面轮廓会越发张开和平坦，入射光经过透镜出射面形成聚焦的 −1 级衍射发生的偏折也越小，满足能量提升效果的闪耀结构高度越大。同时也可以看出，焦点位置均会随着闪耀结构的构建而发生不同程度的偏移，偏移量 <5%。

3.2　闪耀结构数量及位置的影响

透镜结构不同光栅区域的倾斜程度不同，不同区域的闪耀结构对于光束能量提升的贡献度也不同。设定 $f=6$ μm，选取 $m=30$ 的透镜，于底部 (bottom)、中部

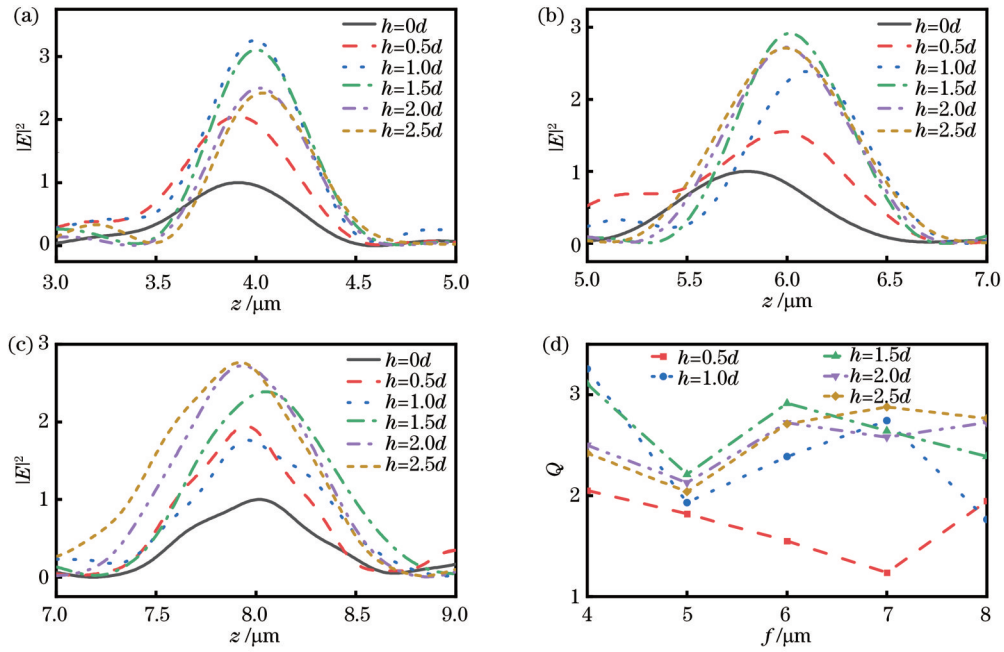图 3 不同焦距下焦场能量与闪耀结构高度的关系。(a) $f=4$ μm；(b) $f=6$ μm；(c) $f=8$ μm；(d) 不同焦距下增强因子 Q 随闪耀结构高度的变化

Fig. 3 Relationship between focal field energy and height of blazed structure at different focal lengths. (a) $f=4$ μm; (b) $f=6$ μm; (c) $f=8$ μm; (d) relationship between enhancement factor Q and height of blazed structure

表 1 不同预设焦距对应的 Q_{max} 及其闪耀结构高度 h

Table 1 Q_{max} corresponding to different preset focal lengths and its blazed structure height h

f /μm	h /μm	Q_{max}
4	$1.0d$	3.26
5	$1.5d$	2.21
6	$1.5d$	2.91
7	$2.5d$	2.87
8	$2.5d$	2.76

（mid）以及顶部（top）位置分别构建数量为 10 和 20 的闪耀结构，进行焦场分析，不同情况的透镜归一化电场分布如图 4 所示。

图 4（a）为构建 10 个闪耀结构的归一化电场分布。底部和顶部区域优化后的焦点位置相对预设焦距有偏移，焦场次级焦点较多；底部区域优化后的焦场能量明显高于中部和顶部。图 4（b）为构建 20 个闪耀结构的归一化电场分布，相较于图 4（a），其焦点的偏移程度较小，次级焦点较少；不同区域优化带来的焦场能量增强也更加接近。

结果表明，闪耀结构构建数量较少时，其构建位置产生的焦场增强效果和对焦场质量的影响存在明显的差异性，底部构建对焦场能量增强的效果最佳，但焦点位置的准确度、次级焦点的抑制能力等表现都较差。随着闪耀结构数量增多，经过闪耀结构调制的衍射光束相互作用，抵消部分相位差，减少焦点偏移。闪耀结构数量较多时，在不同区域的构建也可平衡透镜不同区域的出射光束对焦场的能量贡献。当闪耀结构完全布满透镜出射面时，焦场的能量最大，焦点位置最优。
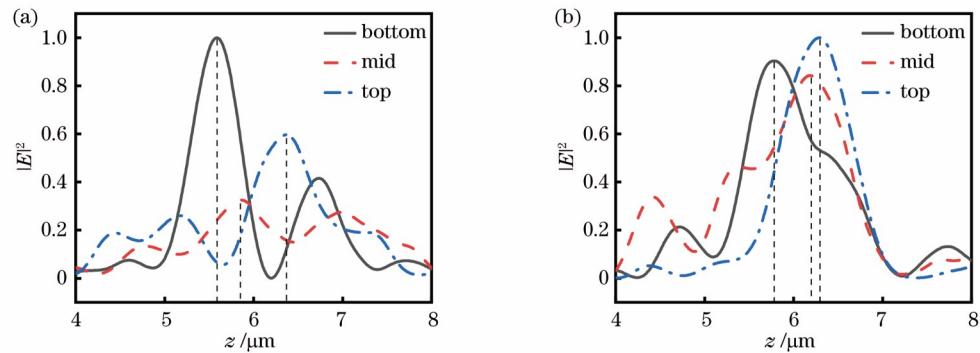

图 4 不同区域构建闪耀结构的焦场归一化电场强度沿纵向分布。闪耀结构数量分别为 (a) 10；(b) 20

Fig. 4 Normalized electric field intensity distribution of focal field along longitudinal direction for constructing blazed structures in different regions. Number of blazed structure is (a) 10; (b) 20

当闪耀结构构建数量有所控制时,少量构建和多量构建,其构建位置产生的不同效果也为焦场调控的设计提供了多样化的选择。

闪耀型亚波长光栅透镜可采用三维光刻技术对材料进行逐层加工,完成制备[26]。电磁波调控机制和结构设计均具有缩放性质,结构设计的思路和调控方案可拓展至各个波段,在长波长情况下,结构的单元尺度较大,对精度要求也较低,将更具制备的可行性。
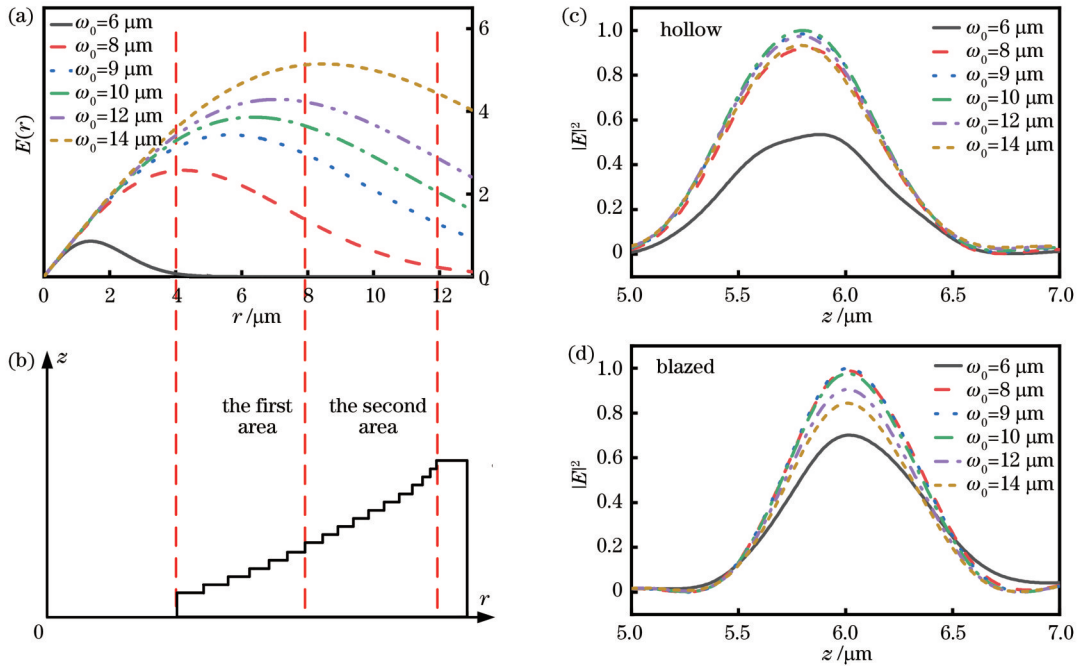
4 入射光参数对焦场的调控

平凹镜经过闪耀结构修饰和优化将有效提升焦场

的聚焦能量,结构确定后,入射光参数的灵活调控也将影响焦场的聚焦效果。调控柱矢量光束的振幅分布和偏振组分,均能实现焦场的动态调控。

4.1 调节振幅实现对焦场的调控

将径向偏振光的振幅调控描述为高斯型:

$$E_r(r) = r \cdot \exp\left[-\left(\frac{r}{w_0}\right)^2\right], \quad (5)$$

式中,w_0 为高斯分布的形状参数,调节 w_0 可以动态调整入射光振幅分布,图 5 为焦场的调控效果。

图 5 入射光振幅对焦场的调控。(a) 高斯径向偏振光振幅与 w_0 的关系;(b) 光栅透镜区域划分示意图;(c) 中空型透镜焦场归一化电场强度沿纵向分布;(d) 闪耀型透镜焦场归一化电场强度沿纵向分布

Fig. 5 Manipulation of focal field by amplitude of incident light. (a) Relationship between Gaussian radially polarized light amplitude and w_0; (b) schematic diagram of grating lens area division; (c) normalized distribution of electric field intensity along longitudinal direction of focal field through hollow lens; (d) normalized distribution of electric field intensity along longitudinal direction of focal field through blazed lens

图 5(a) 为高斯径向偏振光振幅与 w_0 的关系曲线。随着 w_0 的增加,高斯光束的振幅提升,入射区域半径变大。根据式(3)判断,光栅阶梯次序 k 越大,光栅阶梯面越窄,出射面轮廓越陡峭。相同的阶梯个数由于倾角的变化导致入射光贡献面积的不同以及-1级衍射光出射角度不同,对焦场的能量贡献也不同。因此,当光栅周期 l_k 最接近 $(l_1 + l_m)/2$ 时,以此光栅阶梯的顶端为分界线,将透镜出射面分为第一光栅区和第二光栅区,如图 5(b) 所示。图 5(c) 和 5(d) 分别为中空型和闪耀型透镜归一化焦场随 w_0 的变化。当未构建闪耀结构[图 5(c)]且 $w_0 = 6$ μm 时,焦场能量较小;w_0 从 6 μm变化至 10 μm 时,焦场能量递增;w_0 继续增大至 14 μm时,焦场能量趋于平稳甚至减弱。构建闪耀结构后[图

5(d)],当 $w_0 = 6$ μm 时的焦场能量明显高于图 5(c),其他焦场能量变化规律与中空型透镜基本一致。

根据透镜结构轮廓特征和衍射机制分析,当入射光能量贡献于透镜第一光栅区占比大于第二光栅区时,由于光束通过第一光栅区的偏折角度小,光栅的衍射效率高,电场强度随着 w_0 递增。入射光能量贡献于第二光栅区超过第一光栅区时,光栅衍射效率降低,随着 w_0 的增加,电场强度趋于稳定甚至会衰弱。若 w_0 取值过小,入射光大部分经过平凹镜底部的圆孔出射,焦场能量低。若 w_0 取值过大,入射光会有一定比例从阶梯光栅区范围之外出射,导致能量浪费。因此在透镜的结构尺寸固定时,选取合适的 w_0 参数对高斯径向偏振光的振幅和入射区域进行调整,能够有效提升焦场
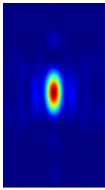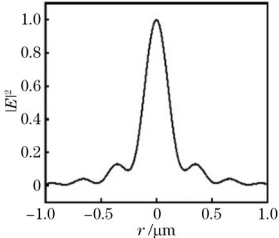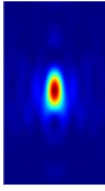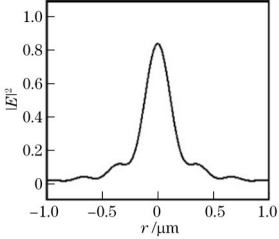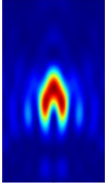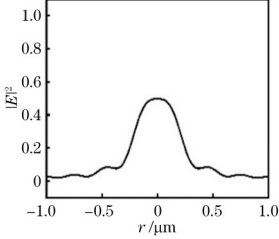
的能量使用效率,获得较高能量的焦场。

4.2 柱矢量光偏振组分对焦场形貌的影响

亚波长光栅透镜能够同时聚焦径向和旋向的偏振分量,充分利用了透镜对于偏振的无依赖性[27]。通过改变柱矢量光偏振组分可以直接调制焦场,设置五组偏振组分比例,聚焦结果如表 2 所示。

表 2 偏振组分对焦场的调控效果

Table 2 Modulation effects of polarization components on focal field

Polarization ratio ($E_r:E_\Phi$)	Morphology of focal field	Focal field intensity distributed along transverse direction
1.0:0.0		
0.7:0.3		
0.5:0.5		
0.3:0.7		
0.0:1.0		

当 $E_r:E_\Phi=1:0$ 时,入射光为纯径向偏振光,出射场横向分量向纵向分量偏折转化,纵向分量在轴上相互叠加,横向分量在轴上相互抵消,焦斑呈实心单焦点,焦点的横向半峰全宽为 $0.457\lambda_0$;当 $E_r:E_\Phi=0:1$ 时,入射光为纯旋向偏振光,出射光束无纵向分量,只有旋向分量,焦斑呈"甜甜圈"形,焦点的横向半峰全宽为 $0.336\lambda_0$;当 $E_r:E_\Phi=0.5:0.5$ 时,此时 CVBs 偏振为径向和旋向偏振光的等比例线性叠加,焦场也为二者焦场的叠加,实心的焦点和空心的"甜甜圈"叠加,由于径向和旋向偏振光入射形成的焦点纵向位置不同,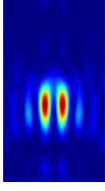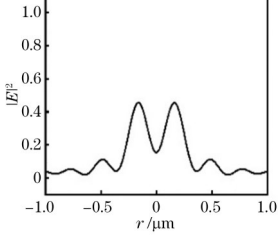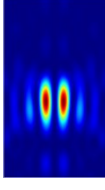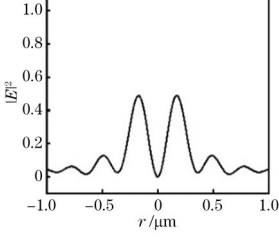焦斑呈"火箭"形,焦点横向半峰全宽为 $0.851\lambda_0$。因此当径向偏振分量超过旋向偏振分量时,焦点的横向半峰全宽可以在 243.8 nm($0.457\lambda_0$,1:0)到 453.3 nm($0.851\lambda_0$,0.5:0.5)之间自由调制。除此之外,当 $E_r:E_\Phi=0.3:0.7$ 时,焦斑呈"纺锤"形。因此,当结构设计确定后,通过调整 CVBs 偏振组分,可实现多样化形状的焦场的动态调控。

5 结 论

本文对亚波长光栅透镜的聚焦性能进行优化,设计了一种闪耀型亚波长光栅透镜,提升了 −1 级衍射光的衍射效率,增强了透镜的焦场能量。研究了闪耀结构的高度以及构建数量和位置对聚焦的影响。结果表明,随着预设焦距的增加,满足透镜最大衍射效率的闪耀结构高度也在增加。当修饰透镜的闪耀结构数量增多时,不同区域的出射光束的能量越均衡,焦场能量越大;同时焦场抑制次级焦点的能力越强,焦点位置越精确。进一步地,探索了入射光分布对透镜聚焦的影响。通过调节高斯径向偏振光的形状参数改变光束的振幅和入射区域半径,实现了焦场能量的动态调控。此外,改变 CVBs 的偏振组分能够实现聚焦的横向调制,获得多样化形貌的焦场。本文研究结果为亚波长光栅透镜的聚焦性能优化提供了思路,并且在光学微操纵、超分辨率成像等方面具有潜在的应用价值。

参 考 文 献

[1] Shvedov V, Davoyan A R, Hnatovsky C, et al. A long-range polarization-controlled optical tractor beam[J]. Nature Photonics, 2014, 8(11): 846-850.

[2] Li M M, Yan S H, Liang Y S, et al. Transverse spinning of particles in highly focused vector vortex beams[J]. Physical Review A, 2017, 95(5): 053802.

[3] Zhang Y Q, Shen J F, Min C J, et al. Nonlinearity-induced multiplexed optical trapping and manipulation with femtosecond vector beams[J]. Nano Letters, 2018, 18(9): 5538-5543.

[4] Gu M, Li X P, Cao Y Y. Optical storage arrays: a perspective for future big data storage[J]. Light: Science & Applications, 2014, 3(5): e177.

[5] Li X P, Cao Y Y, Tian N, et al. Multifocal optical nanoscopy for big data recording at 30 TB capacity and gigabits/second data rate[J]. Optica, 2015, 2(6): 567-570.

[6] Cheng H C, Li P, Liu S, et al. Vortex-controlled morphology conversion of microstructures on silicon induced by femtosecond

vector vortex beams[J]. Applied Physics Letters, 2017, 111(14): 141901.

[7] Meier M, Romano V, Feurer T. Material processing with pulsed radially and azimuthally polarized laser radiation[J]. Applied Physics A, 2007, 86(3): 329-334.

[8] Liu M, Lei Y Z, Yu L, et al. Super-resolution optical microscopy using cylindrical vector beams[J]. Nanophotonics, 2022, 11(15): 3395-3420.

[9] Bautista G, Kakko J P, Dhaka V, et al. Nonlinear microscopy using cylindrical vector beams: applications to three-dimensional imaging of nanostructures[J]. Optics Express, 2017, 25(11): 12463-12468.

[10] Jiang R H, Chen C, Lin D Z, et al. Near-field plasmonic probe with super resolution and high throughput and signal-to-noise ratio[J]. Nano Letters, 2018, 18(2): 881-885.

[11] Totorica S R, Abel T, Fiuza F. Particle acceleration in laser-driven magnetic reconnection[J]. Physics of Plasmas, 2017, 24(4): 041408.

[12] Xu J, Yang Z J, Li J X, et al. Electron acceleration by a tightly focused cylindrical vector Gaussian beam[J]. Laser Physics Letters, 2017, 14(2): 025301.

[13] Chen W B, Zhan Q W. Three-dimensional focus shaping with cylindrical vector beams[J]. Optics Communications, 2006, 265(2): 411-417.

[14] Ko H, Kim H C, Cheng M S. Light focusing at metallic annular slit structure coated with dielectric layers[J]. Applied Optics, 2010, 49(6): 950-954.

[15] Yu Y T, Zappe H. Effect of lens size on the focusing performance of plasmonic lenses and suggestions for the design[J]. Optics Express, 2011, 19(10): 9434-9444.

[16] 仲义, 许吉, 陆云清, 等. 基于一维金属光子晶体平凹镜的柱矢量光束亚波长聚焦[J]. 物理学报, 2014, 63(23): 237801.
Zhong Y, Xu J, Lu Y Q, et al. Subwavelength focusing of cylindrical vector beams by plano-concave lens based on one dimensional metallic photonic crystal[J]. Acta Physica Sinica, 2014, 63(23): 237801.

[17] Wang Z X, Ren G B, Gao Y X, et al. Plasmonic in-plane total internal reflection: azimuthal polarized beam focusing and application[J]. Optics Express, 2017, 25(20): 23989-24000.

[18] Shibata K, Uemoto M. One-dimensional subwavelength position determination exploiting off-axis parabolic mirror[J]. Applied Physics Express, 2017, 10(6): 062501.

[19] Zhu J L, Jin R C, Tang L L, et al. Multidimensional trapping by dual-focusing cylindrical vector beams with all-silicon metalens[J]. Photonics Research, 2022, 10(5): 1162-1169.

[20] Zheng C L, Li J, Wang G C, et al. Fine manipulation of terahertz waves via all-silicon metasurfaces with an independent amplitude and phase[J]. Nanoscale, 2021, 13(11): 5809-5816.

[21] 刘山峰, 袁沭娟, 孙钰淇, 等. 亚波长光栅负折射透镜的柱矢量光束聚焦特性[J]. 光学学报, 2019, 39(11): 1105001.
Liu S F, Yuan S J, Sun Y Q, et al. Focusing properties of cylindrical vector beams through subwavelength grating lenses with negative refractive indices[J]. Acta Optica Sinica, 2019, 39(11): 1105001.

[22] Wang S M, Xu J, Zhong Y, et al. Focus modulation of cylindrical vector beams through negative-index grating lenses[J]. Optics Communications, 2016, 372: 245-249.

[23] Chen M L, Zhu C Y, Huang H S, et al. Focusing characteristics of cylindrical vector beams through a multi-focal all-dielectric grating lens[J]. Optics Letters, 2022, 47(2): 253-256.

[24] Ke L, Li C X, Zhang S M, et al. Tight focusing field of cylindrical vector beams based on cascaded low-refractive index metamaterials[J]. Nanophotonics, 2023, 12(18): 3563-3578.

[25] Gao J, Chen P, Wu L, et al. A review on fabrication of blazed gratings[J]. Journal of Physics D: Applied Physics, 2021, 54(31): 313001.

[26] 王虎. 全息微立体光刻方法研究[D]. 成都: 中国科学院光电技术研究所, 2022: 7-13.
Wang H. Study on holographic micro-stereo lithography method[D]. Chengdu: Institute of Optics and Electronics, Chinese Academy of Sciences, 2022: 7-13.

[27] Zhan Q W. Cylindrical vector beams: from mathematical concepts to applications[J]. Advances in Optics and Photonics, 2009, 1(1): 1-57.

Focusing Optimization and Control of Cylindrical Vector Beams with Blazed Subwavelength Grating Lens

Wang Jun[1], Xu Ji[1*], Li Sheng[1], Chi Tiantian[1], Yao Han[1], Zhang Baifu[2], Liu Ning[1]

[1]College of Electronic and Optical Engineering & College of Flexible Electronics (Future Technology), Nanjing University of Posts and Telecommunications, Nanjing 210023, Jiangsu, China;

[2]School of Electronic and Optical Engineering, Nanjing University of Science and Technology, Nanjing 210023, Jiangsu, China

Abstract

Objective　　The amplitude and polarization of cylindrical vector beams (CVBs) are distributed cylindrically and symmetrically, and the tight CVBs focusing plays an important role in optical micromanipulation, optical storage, laser micromachining, super-resolution imaging, particle acceleration, and other fields. At present, various focusing methods have been developed, such as traditional lenses, plasmonic lenses, negative refractive photonic crystal lenses, parabolic mirrors, and meta-lenses. However, there are limitations including diffraction limit, polarization dependence, and complex preparation. Subwavelength grating lens based on −1st order diffraction can achieve tight focusing of radial and azimuthal polarized lights spontaneously, breaking through the diffraction limit and realizing flexible focal field manipulation. Despite these advantages, the energy efficiency of its focal field still deserves further improvement.

Therefore, we explore and propose a structural optimization scheme for a blazed subwavelength grating lens that can increase the energy ratio of －1st order diffracted light energy to enhance the focal field energy.

Method　We employ the full vector calculation of electromagnetic field (COMSOL Multiphysics software) based on the finite element method (FEM) to carry out specific research. The blazed structure is located on each grating step with a consistent height, and the overall lens structure is a uniform dielectric GaN. Firstly, an equivalent triangular prism model is built to verify the enhancement effect of the blazed structure on － 1st order diffraction. Next, the energy and morphology changes of the focal field before and after modifying the blazed structure are compared, and the influence of the height, number, and location of blazed structures on the focal field is analyzed. Finally, the dynamic manipulation effect of the incident light amplitude distribution and polarization components on the focal field energy and morphology is studied.

Results and discussion　In the equivalent prism model, adding the blazed gratings significantly increases the energy proportion of the -1st order diffracted light, which proves the feasibility of the optimization mechanism (Fig. 1). The hollow grating lens decorated with the blazed structure can significantly increase the focal field energy with the peak value increasing to 2.91 times, while the focusing position is slightly shifted and the focusing width is broadened (Fig. 2). Under different preset focal lengths, the deflection of the beam passing through the lens varies, and the relationship between the focal field energy and the height of the blazed structure also changes. At near and medium focal lengths, the focal field energy first increases and then decreases with the height, and at far focal lengths, the focal field energy increases with the height (Fig. 3). When the number of blazed structures changes, more of them cause the diffracted beams to interact with each other, offset part of the phase difference, and reduce focal shift, with improved focusing energy efficiency (Fig. 4). The incident light distribution can also manipulate the focal field. By controlling the beam parameters to adjust the energy distribution of incident light in various regions of the grating, different diffraction efficiencies of regions are obtained, and the focusing field intensity is controlled (Fig. 5). According to the analysis of lens structural profile characteristics and diffraction mechanisms, when the proportion of incident light energy contributing to the first grating area of the lens is more than that of the second grating area, the grating diffraction efficiency is high and the electric field intensity increases with w_0. When the contribution of incident light energy to the second grating area exceeds the first grating area, the grating diffraction efficiency decreases, and the electric field intensity becomes stable or even weakens with the rising w_0 (Fig. 5). By utilizing the polarization independence of subwavelength grating lenses and adjusting the polarization composition of the incident field, solid single focus, "donut" shaped, "rocket" shaped, and "spindle" shaped focal fields can be obtained (Table 2).

Conclusion　We propose a blazed subwavelength grating lens that can improve the diffraction efficiency of － 1st order diffracted light and enhance the focal field energy of the negative refractive grating lens. As the preset focal length increases, the height of the blazed structure that satisfies the maximum diffraction efficiency of the lens also rises. The increasing number of blazed structures leads to more balanced energy of the outgoing beams in different regions and higher energy of the focal field. Meanwhile, the ability of the focal field to suppress the secondary focus is stronger, and the focal position is more accurate. By adjusting incident Gaussian radially polarized light, the dynamic control of the focal field energy is realized. Changing the polarization components of CVBs can also achieve lateral focusing modulation and obtain focal fields with diverse morphology. Finally, our study provides ideas for optimizing the focusing performance of subwavelength grating lenses and has potential applications in optical micromanipulation, super-resolution imaging, and other fields.

Key words　subwavelength grating lenses; cylindrical vector beams; blazed structure; focusing; regulation